Research Article

Hiroyuki Fukuyama*, Hideo Higashi, Masayoshi Adachi, and Makoto Ohtsuka

Density and surface tension measurements of molten Al–Si based alloys

https://doi.org/10.1515/htmp-2022-0286
received March 30, 2023; accepted August 17, 2023

Abstract: This study is part of a series of studies aimed at measuring the thermophysical properties of molten phase change material-type metallic thermal energy storage materials near 873 K (600°C). The target material is Al–Si based alloys. First, as a feasibility study, density measurements of the molten state of three Al–Si binary alloys (Al–12.2Si, Al–50Si and Al–90Si in atomic%) were performed. A highly accurate non-contact density measurement method based on the static magnetic field superposition electromagnetic levitation (EML) method was employed as the density measurement method. The validity of this experimental method was confirmed, and density of molten Al–Si base alloys (ADC12 and Al–5.9mass%Si–1.6mass%Fe) were measured as a function of temperature with an expanded uncertainty of 1.2%. In addition, the surface tension of the alloys was measured by the droplet oscillation method using the EML technique. The surface tension was successfully obtained as a function of temperature with expanded uncertainty of 2.3%.

Keywords: density, surface tension, Al–Si based alloys, electromagnetic levitation, static magnetic field, droplet oscillation method, Butler model

1 Introduction

To achieve carbon neutrality, it is necessary to further introduce renewable energy sources such as photovoltaic power generation. Carnot batteries (thermal power storage) with large-scale thermal energy storage technology are attracting attention as one means of ensuring a stable energy supply that is not affected by weather conditions, etc. [1,2]. As its heat storage method, latent heat storage is promising because of its features such as high heat storage density and the ability to supply heat at a constant temperature. In Rankine batteries, a type of Carnot battery, the use of high-efficiency steam turbines is a key technology to increase round-trip efficiency. Due to expected vapor temperatures and structural material constraints, phase change materials (PCMs) need to be developed that cover various temperature ranges below 700°C. Shimizu and Nomura [1] have attempted to develop Al–Si–Fe PCMs based on thermodynamic calculation software (Factsage) and thermal analysis. They found an Al–5.9Si–1.6Fe (in mass%) PCM that melted at 846–897 K (573–624°C) and had a high latent heat capacity of 386 $J \cdot g^{-1}$. Kageyama and Morita [3] developed Zn–Al–Mg and Al–Si eutectic alloys as phase-change materials for use in the 300–350°C and 450–550°C temperature ranges, respectively. The problem of reactivity between PCM and the container is another issue that must be solved. Yamanaka et al. [4] have studied the corrosion resistance of Co–Cr–Mo–Si alloys with Al–Si melts at 700°C.

At the same time, to develop a highly efficient heat storage type heat exchanger, it is important to understand the behavior of metal PCM inside the heat exchanger by analyzing its heat storage and release characteristics using numerical simulation techniques for solidification and melting of the metal PCM. For this purpose, thermophysical properties of metal PCM in the molten state are necessary, but it is difficult to measure them with high accuracy, and there are only a few reported cases. In addition, there is of course no data at all on the new PCMs proposed by Shimizu and Nomura [1].

In our laboratory, we are developing a high temperature thermophysical property measurement system (PROSPECT) that can measure thermophysical properties of metals and alloys with high accuracy by combining the electromagnetic levitation (EML) method and static magnetic field [5–14]. In this study, we focus on ADC12 and Al–5.9Si–1.6Fe (in mass%) as metal PCMs and aim to provide the density and surface tension of these alloys in the

* **Corresponding author: Hiroyuki Fukuyama,** Institute of Multidisciplinary Research for Advanced Materials, Tohoku University, 2-1-1 Katahira, Aoba-ku, Sendai, 980-8577 Japan, e-mail: hiroyuki.fukuyama.b6@tohoku.ac.jp
Hideo Higashi, Masayoshi Adachi, Makoto Ohtsuka: Institute of Multidisciplinary Research for Advanced Materials, Tohoku University, 2-1-1 Katahira, Aoba-ku, Sendai, 980-8577 Japan
ORCID: Hiroyuki Fukuyama 0000-0003-0753-4403

molten state as a function of temperature. ADC12 is a type of aluminum alloy commonly used in aluminum die casting, and its composition is shown in Section 2.1. Prior to the measurement of these two alloys, density measurements were first performed on three Al–Si binary alloys (Al–12.2Si, Al–50Si, and Al–90Si in atomic%) as a feasibility study.

2 Experimental

2.1 Samples and differential scanning calorimeter (DSC) measurement

Three types of Al–Si binary alloys (Al–12.2Si, Al–50Si, and Al–90Si in atomic%) were prepared by arc melting after weighing the desired amount of Al (99.99 mass%) and high-purity Si (impurity concentration of O: 10^{16} atoms·cm^{-3}, C: 10^{15} atoms·cm^{-3}).

ADC12 (Fukuoka Alumi Industry Co., Ltd., Japan) and Al–5.9Si–1.6Fe (in mass%) alloy were used in the experiments in this study. The Al–5.9Si–1.6Fe alloy was synthesized from granulated Al (99.5 mass%, Kojundo Chemical Laboratory Co., Ltd. Japan), Si (99.999 mass%, Kojundo Chemical Laboratory Co., Ltd. Japan), and Fe (99.98 mass%, Alfa Aesar, United States) (provided by Dr. Nomura of Hokkaido University) [1]. The chemical compositions of these samples are shown in Table 1.

When measuring sample temperature by the EML method, it is necessary to know the liquidus temperature of the sample in advance because the pyrometer needs to be corrected by the liquidus temperature. Thermal analysis of ADC12 was performed using a DSC (STA449 F3, NETZSCH-Gerätebau GmbH, Germany) to determine the liquidus temperature. Calibration of the DSC was performed in advance using In, Sn, Bi, Al, Ag, and Au as reference materials. The container and lid were made of alumina, and approximately 10 mg of the reference material was placed in the container. The temperature was raised and lowered at 10 K·min^{-1}. Thermal analysis of ADC12 was also performed at the same mass and under the same heating and cooling conditions as the standard samples.

Table 1: Chemical compositions of samples

	Chemical composition (mass%)							
	Al	**Si**	**Fe**	**Cu**	**Mn**	**Mg**	**Zn**	**Ti**
ADC12	Bal.	10.24	0.80	1.89	0.01	0.21	0.48	0.11
Al–5.9Si–1.6Fe	Bal.	5.9	1.6					—

The liquidus temperature of Al–5.9Si–1.6Fe was the reported value (897 K) measured by the same DSC method by Shimizu and Nomura [1].

2.2 Density measurement

For density measurements, the high-temperature thermophysical property measurement system (PROSPECT) developed in our laboratory was used (Figure 1). This system mainly consists of an EML device, a superconducting magnet, a laser for heating, a radiation thermometer, a high-speed camera, and gas supply and exhaust systems. For the EML experiments, the alloys were cut into pieces of about 0.4 g. The sample surfaces were polished to remove the oxide film just prior to experiments. The sample was set in the chamber. The chamber was evacuated to about 1.0×10^{-3} Pa by a turbomolecular pump, and then the chamber was filled with an Ar–5 vol.%H_2 gas mixture that was passed through a magnesium deoxidation column heated at 823 K to reduce the oxygen partial pressure to 10^{-28} atm (10^{-23} Pa). This oxygen partial pressure was measured with an oxygen sensor after Mg deoxidation and before it was introduced into the chamber. The sample was then electromagnetically levitated and melted. The levitation coil used for this measurement is also shown in Figure 1. A coil with high symmetry and a wide coil gap was used for the density measurement, and a tapered coil with high heating efficiency was used for the surface tension measurement.

A superconducting magnet was used to apply a static magnetic field of 2 to 3 T to the levitated sample droplets to suppress their translational motion and surface oscillation. The temperature of the sample droplets was controlled by the heating laser, the current value of the EML coil, and the He gas flow rate blown onto the sample. A semiconductor laser (wavelength of 940 nm; maximum power of 75 W; Hamamatsu Photonics K.K., Japan; SPOLD L12333–511) was used for the heating laser.

The temperature of the sample droplet was measured using a radiation thermometer (temperature range: 450–2,500°C, spectral range: 1.45–1.8 μm; IGA140/MB25, IMPAC Pyrometers, LumaSense Technologies, Germany) from the bottom of the droplet, but measurement was difficult at low temperatures because an oxide film was formed at the bottom of the sample. Therefore, another radiation thermometer (temperature range: 400–3,100°C, wavelength: 1.31 μm; IR-CAQ3CS, CHINO Corporation, Japan) was also installed diagonally above the sample to measure the temperature above the sample. Two optical filters (model number: RSF-25C-1064RU, Sigmakoki Co. Ltd., Japan) were placed in front of

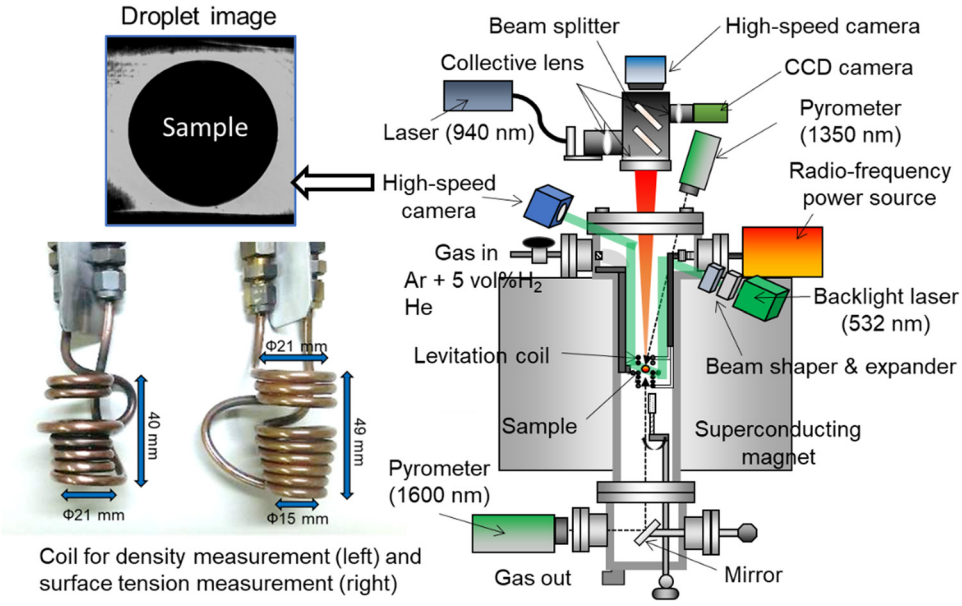

Figure 1: High-temperature thermophysical property measurement system (PROSPECT) for density and surface tension measurements of molten Al–Si based alloy.

the upper radiation thermometer to prevent influence from the heating laser on the upper radiation thermometer. Temperature calibration was performed using the liquidus temperature of both samples, and temperatures were evaluated assuming constant spectral emissivity at the measurement wavelength of the radiation thermometer at temperatures other than the liquidus temperature.

To capture the projected image of the sample droplet, a YAG laser (532 nm) was irradiated horizontally onto the droplet and the projected image of the droplet was acquired using a high-speed camera (frame rate: 500 fps, acquisition time: 10 s). Each image was recorded with a resolution of 500 × 500 pixels as shown in Figure 1.

Assuming that the droplet was vertically axisymmetric, the volume was determined from the obtained images [5–9]. After measuring the projected image of the droplet, the length per pixel was determined by taking nine images of a stainless-steel reference sphere with a diameter of 7.0 mm near the sample levitation position at room temperature. The droplet radius $r(\theta)$ was obtained by fitting the droplet edges using the Legendre polynomial ($P_n(x)$ up to $n = 5$) with coefficient a_n:

$$r(\theta) = \sum_{n=0}^{5} a_n P_n(\cos\,\theta). \tag{1}$$

The sample volume V was obtained from equation (2) assuming that the sample shape was rotationally symmetric around a vertical axis.

$$V = \frac{2\pi}{3}\int_{-1}^{1} r^3(\theta) d\,\cos(\theta). \tag{2}$$

The mass of the sample was measured using an electronic balance before and after the levitation experiment, and the average value was used. Density was determined from the volume and mass obtained.

2.3 Surface tension measurement

Surface tension was determined by the droplet oscillation method [5]. For droplets levitated by electromagnetic forces under gravity, the surface tension (σ) was determined from the Rayleigh equation as modified by Cummings and Blackburn [15–17]:

$$\sigma = \frac{3\pi}{8} M \nu_R^2, \tag{3}$$

$$\nu_R^2 = \frac{1}{5}\sum_{m=-2}^{2} \nu_{2,m}^2 - \nu_t^2\left\{1.9 + 1.2\left(\frac{g}{8\pi^2\nu_t^2 r}\right)^2\right\}, \tag{4}$$

$$\nu_t^2 = \frac{1}{3}\sum_{m=-1}^{1} \nu_{1,m}^2, \tag{5}$$

where M is the mass of the sample, g is the acceleration of gravity, and r is the radius of the sample. The value of r was calculated from density data assuming the droplet to be spherical. $\nu_{2,m}$ is the frequency of surface oscillation

with m = 0, ±1, or ±2 for the l = 2 mode, and ν_t is the frequency of the translational motion of the center of gravity consisting of m = 0 and ±1 oscillations for l = 1 mode. The time series data G_x, G_y and G_z representing the horizontal (x, y) and vertical (z) displacements of the center of gravity were Fast Fourier Transformed (FFT) to obtain the ν_t values. Here, the frequency of G_z was the same as the frequency of the area of the sample images taken from the top view camera. The values of $\nu_{2,m}$ were obtained by FFT of the R+ and R– time series data. Here, $R+ = R_x + R_y$ and $R- = R_x - R_y$, where R_x and R_y are the radii along the x- and y-axes of the sample images, respectively. Frequency peaks were assigned according to the rule that m = 0 is a mode that appears only in the R+ spectrum, $m = \pm 2$ is a mode that appears only in the R– spectrum, and $m = \pm 1$ is a mode that appears in both the R+ and R– spectrum.

The sample was kept at a constant temperature without applying a static magnetic field, and the oscillation of the droplet was recorded by a high-speed camera from the vertical direction at frame rate of 500–125 fps for 10 s. When measuring surface tension, the optical system above the sample was removed and only a high-speed camera and a condenser lens were installed directly on the sample to increase the amount of light radiated from the sample, allowing the observation of droplet oscillations as low as 930 K. The temperature of the sample was controlled by the current value to the EML coil and the He gas flow rate. By fast Fourier transforming the droplet image, the frequency of the translational motion of the droplet's center of gravity and the frequency of the droplet's surface oscillation were obtained.

3 Results

3.1 Liquidus temperature

Figure 2 shows the results of DSC measurement of ADC12. A large endothermic peak was observed during the temperature increase, and the endset temperature was found to be around 865 K (592°C). Eight samples were used, and the endset temperature was measured four times repeatedly per sample. The average of all values was taken, and the liquidus temperature (T_L) of ADC12 was determined to be 865 K. The liquidus temperature of Al–5.9Si–1.6Fe was reported to be 897 K by Shimizu and Nomura [1].

3.2 Density

Figure 3 shows an example of temperature variation when the density of molten Al–5.9Si–1.6Fe alloy was measured. After the temperature calibration of the radiation thermometer was performed at the liquidus temperature, the temperature of the droplet was stabilized by heating it with a laser and holding it for a certain time. After that, the laser power was gradually decreased and the droplet was cooled with He gas, and the temperature of the droplet was lowered in a stepwise manner. Below about 1,380 K, a thin oxide film was formed in the lower part of the droplet, but the oxide film did not cover the entire droplet and remained in the lower part, so the measurement was continued.

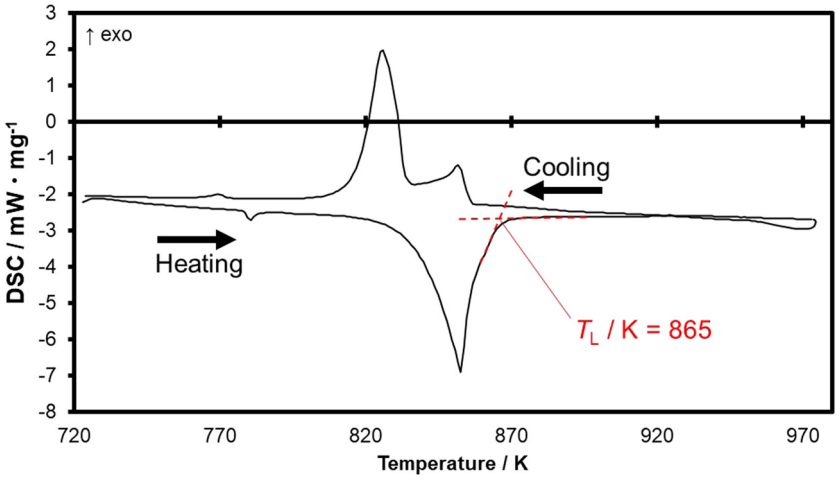

Figure 2: DSC profile for ADC12.

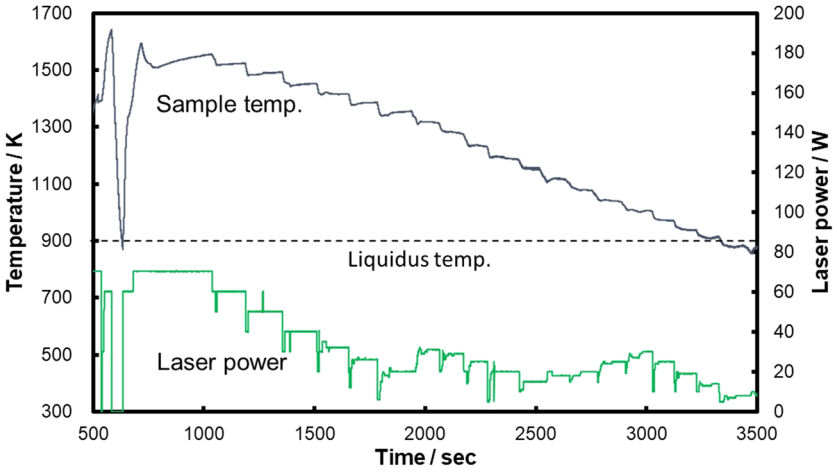

Figure 3: Temperature variation for the density measurement of molten Al–5.9Si–1.6Fe alloy.

Figure 4 shows the temperature dependence of the density of ADC12, Al–5.9Si–1.6Fe, and three Al–Si binary alloys in the molten state. The densities of these alloys all show a negative temperature dependence and are given in the form of the following equation.

$$\rho/\mathrm{kg{\cdot}m^{-3}} = \rho_{\mathrm{L}} + \rho_{\mathrm{T}}(T - T_{\mathrm{L}}), \tag{6}$$

where ρ_{L} is the value of density at the liquidus temperature and ρ_{T} is the temperature coefficient. Table 2 shows the values of these parameters obtained by linear regression of the experimental results. The expanded uncertainty is 1.2%, which is explained in the Discussion.

The figure shows the recommended density values for pure Al reviewed by Assael et al. [18] together with the density of pure Si measured by Mizuno et al. [19] using the EML method with a static magnetic field and the results for Al–Si alloys measured by Schmitz et al. [20] using the EML method. The composition dependence of these data is discussed in terms of molar volume in the Discussion.

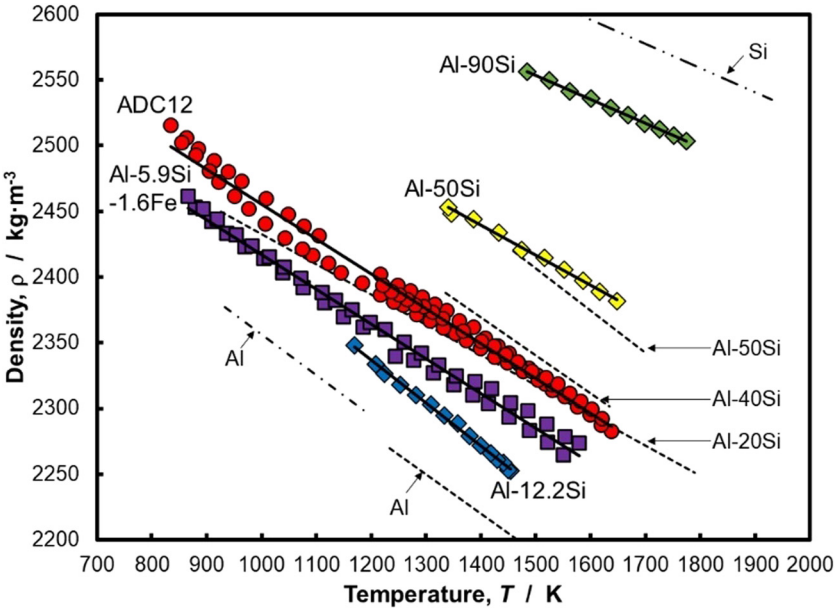

Figure 4: Temperature dependence of the density of ADC12 (red circle), Al–5.9Si–1.6Fe (violet square), and three Al–Si binary alloys (Al–12.2Si (blue diamond), Al–50Si (yellow diamond), and Al–90Si (green diamond)) in the molten state. Literature data: density of Al recommended by Assael et al. [18] (dash-dot-dash line), Si reported by Mizuno et al. [19] (dashed-two dotted line), and Al–Si alloys reported by Schmitz et al. [20] (dotted line).

Table 2: Summary of the density of Al–Si based alloys measured in this study in the molten state

Sample	Liquidus temp. T_L/K	Density at T_L ρ_L/kg·m^{-3}	Temp. coefficient ρ_T/kg·m^{-3}·K^{-1}	Temp. range/K
ADC12	865	2,492	−0.2652	835–1,639
Al–5.9Si–1.6Fe	897	2,448	−0.2647	866–1,580
Al–12.2Si (at%)	850	2,451	−0.3263	1,169–1,454
Al–50Si (at%)	1,334	2,455	−0.2274	1,340–1,648
Al–90Si (at%)	1,663	2,524	−0.1825	1,485–1,774

Liquidus temperatures for the Al–5.9Si–1.6Fe alloy were taken from the data of Shimizu and Nomura [1], while those for the Al–Si alloy were read from the phase diagram [21].

3.3 Surface tension

Similar to the density measurement, the surface tension measurement was performed by heating and holding the sample uniformly melted, then lowering the sample temperature in a stepwise manner while measuring the oscillation of the droplets with a high-speed camera. Figure 5 shows an example of peak identification based on the fast Fourier transform of the center-of-gravity shift and surface oscillation of molten Al–5.9Si–1.6Fe.

The results of surface tension measurements of molten ADC12 and Al–5.9Si–1.6Fe are shown in Figure 6. The surface tension was found to have a negative temperature dependence over the measurement temperature range. The least-squares approximation of the temperature dependence as a linear function of temperature is expressed by the following equation.

$$\sigma/\mathrm{mN\cdot m^{-1}} = \sigma_L + \sigma_T(T - T_L), \tag{7}$$

where σ_L is the value of surface tension at the liquidus temperature and σ_T is the temperature coefficient. Table 3 shows the values of these parameters. The expanded uncertainty is 2.3%, which is explained in the Discussion.

The figure also shows the surface tension of Al–Si alloys measured by the droplet oscillation method using the EML method by Kobatake et al. [22] and by the sessile drop method using graphite substrates by Dou et al. [23] and by the sessile drop method using Al_2O_3 substrates by Takahashi et al. [24]. The sessile drop method with different substrates shows significantly different values. This may be due to the interfacial reaction between the substrate and the droplet. The results of this study and those of Kobatake et al. [22] are discussed in terms of composition dependence, which is discussed in the Discussion.

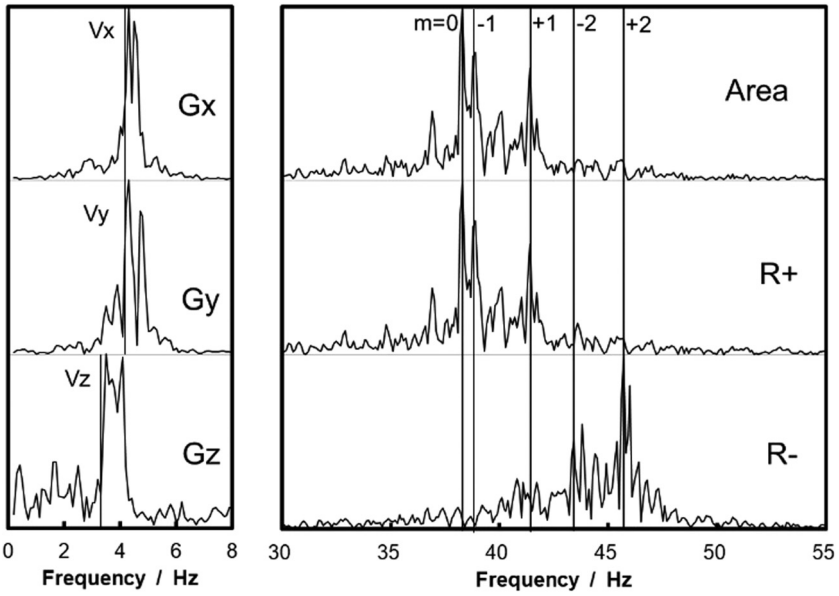

Figure 5: An example of center-of-gravity translation frequency (left) and surface oscillation frequency (right) of Al–5.9Si–1.6Fe (sample mass: 0.4433 g) at 1,128 K.

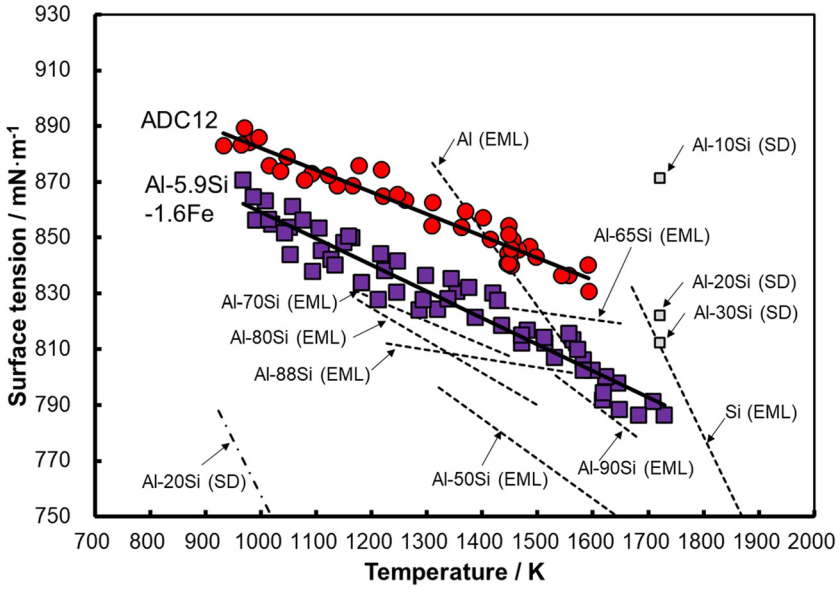

Figure 6: Temperature dependence of the surface tension of ADC12 (red circle) and Al–5.9Si–1.6Fe (violet square) in the molten state. Literature data: surface tension of Al–Si alloys measured by EML method by Kobatake et al. [22] (dotted line), Al–20Si measured by sessile drop method using graphite substrate by Dou et al. [23] (dash-dot-dash line), and Al–Si alloys measured by sessile drop method using Al_2O_3 substrate by Takahashi et al. [24] (grey square).

4 Discussion

4.1 Compositional dependence of molar volume

Schmitz et al. [20] measured the density of molten Al–Si alloys of various compositions as a function of temperature and composition up to a Si concentration of 50 at% using the EML method. Since the ADC12 and Al–5.9Si–1.6Fe we measured in this study are Al–Si–Cu ternary alloy and Al–Si–Fe ternary alloy (see Table 1), direct comparison is difficult. Here, the molar volumes of molten ADC12 and Al–5.9Si–1.6Fe were calculated as an Al–Si binary system and compared with the results of Schmitz et al. Figure 7 shows the Si concentration dependence of the molar volume of molten Al–Si binary alloy at 1,400 and 1,600 K. The molar volume was calculated using the recommended density data for pure Al as reviewed by Assael et al. [18]. The molar volume of pure Si was calculated using the density data measured by Mizuno et al. [19] using the EML method under a static magnetic field. The results of Al–Si binary alloys including this study and Schmitz' data almost followed the ideal solution model, while the results for ADC12 and Al–5.9Si–1.6Fe alloys deviated negatively from the ideal solution model. The molar volume deviation by 3–4% is considered to be due to the influence of 1.89% Cu in ADC12 and 1.6% Fe in Al–5.9Si–1.6Fe.

4.2 Compositional dependence of surface tension

Figure 8 shows the composition dependence of the surface tension of Al–Si binary alloys at 1,400 and 1,600 K. The data for ADC12 and Al–5.9Si–1.6Fe alloys obtained in this study are plotted in the same figure as the Al–Si binary system. The experimental results measured by Kobatake et al. [22] at various compositions are also plotted.

According to the Butler model [25,26], the surface tension of an Al–Si melt is given by equation (8) or equation (9).

Table 3: Summary of the surface tension of Al–Si based alloys measured in this study in the molten state

Sample	Liquidus temp. T_L/K	Density at T_L σ_L/mN·m^{-1}	Temp. coefficient σ_T/mN·m^{-1}·K^{-1}	Temp. range/K
ADC12	865	893	−0.0786	932–1,593
Al–5.9Si–1.6Fe	897	869	−0.0947	969–1,729

Liquidus temperatures for the Al–5.9Si–1.6Fe alloy were taken from the data of Shimizu and Nomura [1].

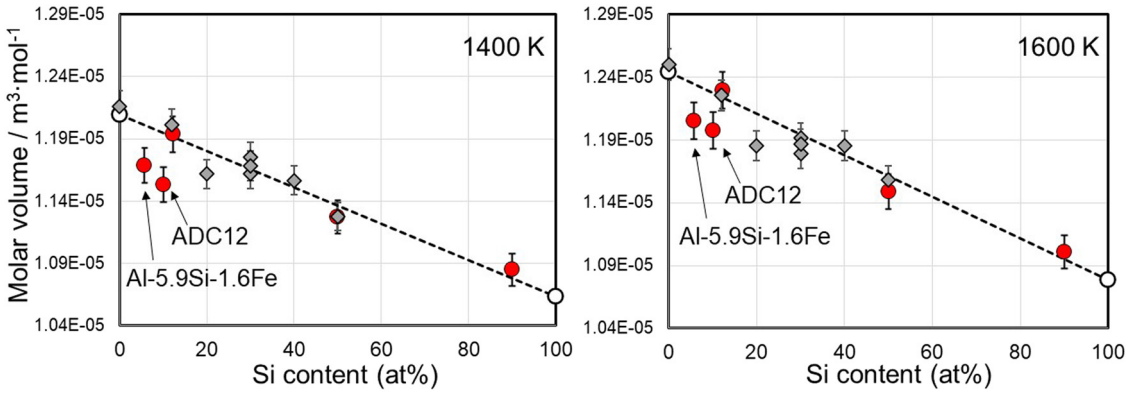

Figure 7: Compositional dependence of the molar volume of molten Al–Si binary alloy at 1,400 and 1,600 K. This study (red circle), Schmitz et al. [20] (grey diamond), pure Al [18] and pure Si [19] (open circles), and ideal solution approximation (dashed lines).

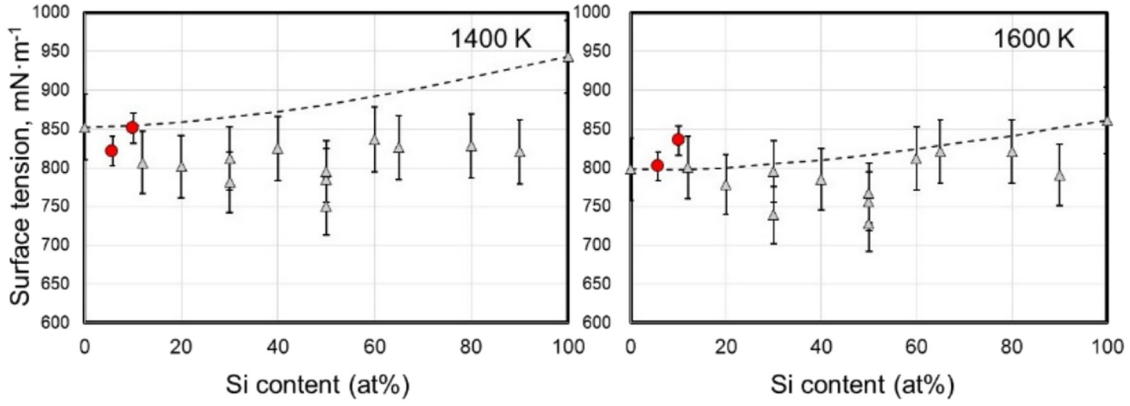

Figure 8: Compositional dependence of the surface tension of molten Al–Si binary alloy at 1,400 and 1,600 K. This study (red circle), Kobatake et al. [22] (grey triangle), and Butler model (dashed lines).

$$\sigma = \sigma_{Al} + \frac{RT}{A_{Al}}\ln\frac{(1 - N_{Si}^{s})}{(1 - N_{Si})} + \frac{1}{A_{Al}}(G_{Al}^{ex,s} - G_{Al}^{ex}), \quad (8)$$

$$\sigma = \sigma_{Si} + \frac{RT}{A_{Si}}\ln\frac{N_{Si}^{s}}{N_{Si}} + \frac{1}{A_{Si}}(G_{Si}^{ex,s} - G_{Si}^{ex}), \quad (9)$$

where R is the gas constant, and σ_X, N_X, and G_X^{ex} are the surface tension, mole fraction, and partial molar excess Gibbs energy of X (= Al or Si), respectively. A_X represents the surface area in a monolayer of pure liquid X, which is given by equation (10) using Avogadro constant (N_o), molar volume of X (V_X) and constant L.

$$A_X = LN_0^{1/3}V_X^{2/3}, \quad (10)$$

where V_X is obtained from the density of X and the constant L is 1.091, which is used for liquid metals [26]. N_X^s and $G_X^{ex,s}$ represent the molar fraction of X and the partial molar excess Gibbs energy in the hypothetical "surface phase." $G_X^{ex,s}$ is related to G_X^{ex} by the following equation, where the value of β is reported as 0.83 for liquid alloys [26].

$$G_X^{ex,s} = \beta G_X^{ex}. \quad (11)$$

The partial molar excess Gibbs energy is obtained from equations (12) and (13) using the molar excess Gibbs energy of the alloy.

$$G_{Al}^{ex} = G^{ex} - N_{Si}\frac{\partial G^{ex}}{\partial N_{Si}}, \quad (12)$$

Table 4: Parameters used in the Butler model for molten Al–Si alloy

Parameter		Ref
Surface tension of Al, σ_{Al}/mN·m^{-1}	979 − 0.271(T − 933)	[22]
Surface tension of Si, σ_{Si}/mN·m^{-1}	826 − 0.412(T − 1,685)	[22]
Density of Al, ρ_{Al}/kg·m^{-3}	2377.23 − 0.311(T − 933)	[18]
Density of Si, ρ_{Si}/kg·m^{-3}	2,580 − 0.184(T − 1,687)	[19]
L_0/J·mol^{-1}	−11340.1 − 1.23394T	[27]
L_1/J·mol^{-1}	−3530.93 + 1.35993T	[27]
L_2/J·mol^{-1}	2265.39	[27]

Table 5: Uncertainty evaluation in density measurement of Al–5.9Si–1.6Fe at 1,551 K (ρ = 2,265 kg·m^{-3})

Factor	Standard uncertainty u	Sensitivity coefficient	Contribution (kg·m^{-3})
Uncertainty of volume: $u(V)$	$u^2(V) = u_1^2(V) + u_2^2(V)$ 1.18×10^{-9} m^3	$\frac{\partial \rho}{\partial V} = -1.10 \times 10^{10}$ kg·m^{-6}	–12.9
Variation of volume: $u_1(V)$	6.58×10^{-10} m^3	$\frac{\partial \rho}{\partial V} = -1.10 \times 10^{10}$ kg·m^{-6}	–7.2
Conversion from pixels to real length: $u_2(V)$	9.75×10^{-10} m^3	$\frac{\partial \rho}{\partial V} = -1.10 \times 10^{10}$ kg·m^{-6}	–10.7
(Accuracy of micrometer: $u(r)$)	($\frac{1}{\sqrt{3}} \times 10^{-6}$ m)	$\left(\frac{\partial V}{\partial r} = 1.69 \times 10^{-4}\ \text{m}^2\right)$	($u_2(V) = 9.75 \times 10^{-10}$ m^3)
Uncertainty of mass due to evaporation loss: $u(M)$	9.10×10^{-6} kg	$\frac{\partial \rho}{\partial M} = 4.85 \times 10^{6}$ m^{-3}	4.4
Combined standard uncertainty $u(\rho)$			13.6
Expanded uncertainty $U = 2u(\rho)$			27.3 (1.2%)

Table 6: Uncertainty evaluation in surface tension measurement of ADC12 at 1,448 K (σ = 851 mN·m^{-1})

Factor	Standard uncertainty u	Sensitivity coefficient	Contribution (mN·m^{-1})
Uncertainty of oscillation frequency: $u(\sigma_R)$	0.35 Hz	$\frac{\partial \sigma}{\partial \nu_R} = \frac{3\pi M \nu_R}{4} = 4.26 \times 10^{-2}$ N·m^{-1}·s	14.9
Uncertainty of mass due to evaporation loss: $u(M)$	3.67×10^{-6} kg	$\frac{\partial \sigma}{\partial M} = \frac{3\pi \nu_R^2}{8} = 2.03 \times 10^{3}$ N·m^{-1}·kg	7.5
Combined standard uncertainty $u(\sigma)$			16.7
Expanded uncertainty $U = 2u(\sigma)$			33.3 (2.3%)

$$G_{\mathrm{Si}}^{\mathrm{ex}} = G^{\mathrm{ex}} + (1 - N_{\mathrm{Si}})\frac{\partial G^{\mathrm{ex}}}{\partial N_{\mathrm{Si}}}. \quad (13)$$

The molar excess Gibbs energy is given by using the interaction parameters (L_0, L_1 and L_2) of the Redlich-Kister polynomial [27] as follows,

$$G^{\mathrm{ex}} = (1 - N_{\mathrm{Si}})N_{\mathrm{Si}}\{L_0 + (1 - 2N_{\mathrm{Si}})L_1 + (1 - 2N_{\mathrm{Si}})^2 L_2\}. \quad (14)$$

The parameters used in the Butler model are shown in Table 4. Using these parameters, equations (8) and (9) can be solved as simultaneous equations to obtain the composition dependence of surface tension.

The composition dependences calculated by the Butler model are shown as dashed lines at 1,400 and 1,600 K. The results of the Butler model indicate that the Al–Si binary alloy is not a system in which one element is strongly localized on the surface, and that its surface tension has a moderate composition dependence. The data of ADC12 and Al–5.9Si–1.6Fe alloys measured in this study are also consistent with the results of Kobatake et al. [22] and the behavior of the Butler model.

The larger deviation from the Butler model at 1,400 K than at 1,600 K in the Kobatake et al. data [22] is thought to be due to the extrapolation of the surface tension of pure Si to the large undercooling region. Surface active elements such as oxygen greatly affect both the absolute value of the surface tension of molten Si and its temperature coefficient, and this should be considered when extrapolating.

4.3 Uncertainty evaluation in density measurement

An example of uncertainty evaluation in density measurement is shown in Table 5. Among the uncertainty factors, both volume uncertainty ($u(V)$) and mass uncertainty ($u(M)$) contributed significantly to the uncertainty of the density measurement. The expanded uncertainty was estimated to be 1.2%, which is twice the value of the combined standard uncertainty calculated from each uncertainty factor.

4.4 Uncertainty evaluation in surface tension measurement

The uncertainty evaluation in the surface tension measurement is shown in Table 6. The uncertainty of the oscillation frequency was evaluated from the standard deviation of the results of ten measurements made on the same sample and at the same temperature. Among the uncertainty factors, the standard deviation of the oscillation frequency was found to contribute significantly to the overall uncertainty. The expanded uncertainty, which is twice the combined standard uncertainty calculated from each uncertainty factor, was estimated to be 2.3%.

5 Conclusion

In this study, the density and surface tension of Al–Si based alloys in the molten state were measured by EML. During density measurements, a static magnetic field was applied to suppress droplet oscillations. The density of three Al–Si binary alloys (Al–12.2Si, Al–50Si and Al–90Si in atomic%) and an Al–Si base alloy (ADC12 and Al–5.9mass%Si–1.6mass%Fe) were measured as a function of temperature with expanded uncertainty of 1.2%. In addition, the surface tension of the alloys was measured by the droplet oscillation method and obtained as a function of temperature with expanded uncertainty of 2.3%.

Acknowledgement: The authors are grateful to the support from a project, JPNP16002, commissioned by the New Energy and Industrial Technology Development Organization (NEDO).

Funding information: This study was supported by a project, JPNP16002, commissioned by the New Energy and Industrial Technology Development Organization (NEDO).

Author contributions: Hiroyuki Fukuyama: conceptualization, methodology, formal analysis, investigation, resources, data curation, writing, visualization, supervision, project administration, funding acquisition; Hideo Higashi: methodology, investigation, formal analysis, visualization, data curation; Masayoshi Adachi: methodology, investigation, formal analysis, visualization, data curation; Makoto Ohtsuka: methodology, investigation, formal analysis, visualization, data curation.

Conflict of interest: The authors declare no conflict of interest. Hiroyuki Fukuyama serves as the Editor-in-Chief of High Temperature Materials and Processes. However, he was not involved in the review process of this article, which was handled entirely by other Editors of the journal.

Data availability statement: Data would be available with the permission by a project, JPNP16002.

References

[1] Shimizu, Y. and T. Nomura. Al–Si–Fe alloy-based phase change material for high-temperature heat storage. *High Temperature Materials and Processes*, Vol. 42, 2023, id. 20220280.

[2] Okazaki, T. Electric thermal energy storage and advantage of rotating heater having synchronous inertia. *Renewable Energy*, Vol. 151, 2020, pp. 563–574.

[3] Kageyama, Y. and K. Morita. Compositional and thermophysical study of Al–Si- and Zn–Al–Mg-based eutectic alloys for latent heat storage. *High Temperature Materials and Processes*, Vol. 42, 2023, id. 20220269.

[4] Yamanaka, K., M. Mori, K. Yoshida, P. Tunthawiroon, and A. Chiba. Corrosion behavior of a Co–Cr–Mo–Si alloy in pure Al and Al–Si melt. *High Temperature Materials and Processes*, Vol. 42, 2023, id. 20220278

[5] Fukuyama, H., H. Higashi, and H. Yamano. Effect of B_4C addition on the solidus and liquidus temperatures, density and surface tension of type 316 austenitic stainless steel in the liquid state. *Journal of Nuclear Materials*, Vol. 554, 2021, id. 153100.

[6] Fukuyama, H., M. Watanabe, and M. Adachi. Recent studies on thermophysical properties of metallic alloys with PROSPECT: Excess properties to construct a solution model. *High Temperatures-High Pressures*, Vol. 49, 2020, pp. 197–210.

[7] Watanabe, M., M. Adachi, M. Uchikoshi, and H. Fukuyama. Densities of Pt-X (X: Fe, Co, Ni and Cu) binary melts and thermodynamic correlations. *Fluid Phase Equilibria*, Vol. 515, 2020, id. 112596.

[8] Watanabe, M., M. Adachi, and H. Fukuyama. Density measurement of Ti-X (X = Cu, Ni) melts and thermodynamic correlations. *Journal of Materials Science*, Vol. 54, 2019, pp. 4306–4313.

[9] Adachi, M., A. Sato, S. Hamaya, M. Ohtsuka, and H. Fukuyama. Containerless measurements of the liquid-state density of Ni-Al alloys for use as turbine blade materials. *SN Applied Sciences*, Vol. 1, 2019, id. 18.

[10] Adachi, M., Y. Yamagata, M. Watanabe, S. Hamaya, M. Ohtsuka, and H. Fukuyama. Composition dependence of normal spectral emissivity of liquid Ni-Al alloys. *ISIJ International*, Vol. 61, 2021, pp. 684–689.

[11] Watanabe, M., M. Adachi, and H. Fukuyama. Normal spectral emissivity and heat capacity at constant pressure of Fe-Ni melts. *Journal of Materials Science*, Vol. 52, 2017, pp. 9850–9858.

[12] Fukuyama, H., H. Higashi, and H. Yamano. Normal spectral emissivity, specific heat capacity, and thermal conductivity of type 316 austenitic stainless steel containing up to 10 mass% B_4C in a liquid state. *Journal of Nuclear Materials*, Vol. 568, 2022, id. 153865.

[13] Watanabe, M., M. Adachi, and H. Fukuyama. Heat capacities and thermal conductivities of palladium and titanium melts and correlation between thermal diffusivity and density of states for transition metals in a liquid state. *Journal of Molecular Liquids*, Vol. 324, 2021, id. 115138.

[14] Watanabe, M., M. Adachi, M. Uchikoshi, and H. Fukuyama. Thermal conductivities of Fe-Ni melts measured by non-contact laser modulation calorimetry. *Metallurgical and Materials Transactions A: Physical Metallurgy and Materials Science*, Vol. 50A, 2019, pp. 3295–3300.

[15] Brillo, J. *Thermophysical properties of multicomponent liquid alloys*, Walter de Gruyter GmbH, Berlin/Boston, 2016, pp. 28–32.

[16] Rayleigh, L. On the capillary phenomena of jets. *Proceedings of the Royal Society of London (1854–1905), Philosophical Transactions of the Royal Society*, Vol. 29, 1879, id. 71. Royal Society of London.

[17] Cummings, D. L. and D. A. Blackburn. Oscillations of magnetically levitated aspherical droplets. *Journal of Fluid Mechanics*, Vol. 224, 1991, pp. 395–416.

[18] Assael, M. J., K. Kakosimos, R. M. Banish, J. Brillo, I. Egry, R. Brooks, et al. Reference data for the density and viscosity of liquid aluminum and liquid iron. *Journal of Physical and Chemical Reference Data*, Vol. 35, 2006, id. 285.

[19] Mizuno, A., H. Kawauchi, M. Tanno, K. Murai, H. Kobatake, H. Fukuyama, et al. Concentration dependence of molar volume of binary Si alloys in liquid state. *ISIJ International*, Vol. 54, 2014, pp. 2120–2124.

[20] Schmitz, J., B. Hallstedt, J. Brillo, I. Egry, and M. Schick. Density and thermal expansion of liquid Al–Si alloys. *Journal of Materials Science*, Vol. 47, 2012, pp. 3706–3712.
[21] Okamoto, H. *Desk handbook, Phase diagrams for binary alloys*, ASM International, Materials Park, OH, 2000, p. 43.
[22] Kobatake, H., J. Brillo, J. Schmitz, and P. Pichon. Surface tension of binary Al–Si liquid alloys. *Journal of Materials Science*, Vol. 50, 2015, pp. 3351–3360.
[23] Dou, L., Z. Yuan, J. Li, J. Li, and X. Wang. Surface tension of molten Al-Si alloy at temperatures ranging from 923 to 1123 K. *Chinese Science Bulletin*, Vol. 53, 2008, pp. 2593–2598.
[24] Takahashi, M., D. Giuranno, E. Ricci, E. Arato, and R. M. Novakovic. Surface Properties of Liquid Al-Si Alloys. *Metallurgical and Materials Transactions A: Physical Metallurgy and Materials Science*, Vol. 50, 2019, pp. 1050–1060.
[25] Butler, J. A. V. The thermodynamics of the surfaces of solutions. *Proceedings of the Royal Society of London. Series A, Containing Papers of a Mathematical and Physical Character*, Vol. 135, 1932, pp. 348–375.
[26] Tanaka, T., K. Hack, T. Iida, and S. Hara. Application of thermodynamic databases to the evaluation of surface tensions of molten alloys, salt mixtures and oxide mixtures. *Zeitschrift für Metallkunde*, Vol. 87, 1996, pp. 380–389.
[27] Hea, C., Y. Dua, H. Chena, and H. Xua. Experimental investigation and thermodynamic modeling of the Al-Cu-Si system. *CALPHAD*, Vol. 33, 2009, pp. 200–210.